



RESEARCH LETTER

10.1002/2015GL066199

Key Points:

- CAPE in radiative-convective equilibrium depends on the saturation deficit of the troposphere
- Increasing the sea surface temperature increases undilute parcel buoyancy in the upper troposphere
- Reducing the relative humidity increases undilute parcel buoyancy throughout the troposphere

Supporting Information:

- Text S1 and Figure S1 Caption
- Figure S1

Correspondence to:

J. T. Seeley,
jseeley@berkeley.edu

Citation:

Seeley, J. T., and D. M. Romps (2015), Why does tropical convective available potential energy (CAPE) increase with warming?, *Geophys. Res. Lett.*, *42*, 10,429–10,437, doi:10.1002/2015GL066199.

Received 14 SEP 2015

Accepted 10 NOV 2015

Accepted article online 23 NOV 2015

Published online 2 DEC 2015

Why does tropical convective available potential energy (CAPE) increase with warming?

Jacob T. Seeley^{1,2} and David M. Romps^{1,2}

¹Department of Earth and Planetary Science, University of California, Berkeley, California, USA, ²Climate and Ecosystem Sciences Division, Lawrence Berkeley National Laboratory, Berkeley, California, USA

Abstract Recent work has produced a theory for tropical convective available potential energy (CAPE) that highlights the Clausius-Clapeyron (CC) scaling of the atmosphere's saturation deficit as a driver of increases in CAPE with warming. Here we test this so-called "zero-buoyancy" theory for CAPE by modulating the saturation deficit of cloud-resolving simulations of radiative-convective equilibrium in two ways: changing the sea surface temperature (SST) and changing the environmental relative humidity (RH). For earthlike and warmer SSTs, undilute parcel buoyancy in the lower troposphere is insensitive to increasing SST because of a countervailing CC scaling that balances the increase in the saturation deficit; however, buoyancy increases dramatically with SST in the upper troposphere. Conversely, in the RH experiment, undilute buoyancy throughout the troposphere increases monotonically with decreasing RH. We show that the zero-buoyancy theory successfully predicts these contrasting behaviors, building confidence that it describes the fundamental physics of CAPE and its response to warming.

1. Introduction

Convective available potential energy (CAPE), loosely defined as the vertically integrated buoyancy of adiabatically lifted subcloud air, is one of the most elementary concepts in atmospheric science. Weather centers around the world calculate CAPE hundreds of times per hour to forecast atmospheric instability and issue severe storm warnings, drawing on evidence that CAPE is a predictor of thunderstorm severity [Brooks, 1994], lightning flash rates [Williams *et al.*, 1992], precipitation extremes [Lepore *et al.*, 2014], and more. CAPE is fundamental to our understanding of the atmosphere on longer timescales, too: a large majority of deep convective parameterizations in contemporary global climate models (GCMs) rely on CAPE to compute cloud base mass flux, which controls the convective heating and cloud cover in simulations of the coming century's climate [e.g., Lin *et al.*, 2015, Table 2]. The skill of CAPE in predicting today's storms has also led to a number of studies that translate increases in CAPE in GCMs into projected convective hazards in a warmer climate [e.g., Diffenbaugh *et al.*, 2013; Romps *et al.*, 2014; Seeley and Romps, 2015]. Clearly, our simulations of future climate, and many of the warnings about future severe weather drawn from such simulations, depend on the physics of CAPE. What is that physics?

Unfortunately, the current generation of GCMs is run at resolutions too coarse to resolve moist convection, so they are not ideal tools for gaining a process-level understanding of what sets CAPE and why it should increase with global warming. GCMs do, however, show significantly more agreement on future increases in tropical oceanic CAPE than in midlatitude CAPE, which suggests that tropical dynamics are an attractive conceptual starting point [e.g., Sobel and Camargo, 2011; Fasullo, 2011; Seeley and Romps, 2015]. Fortunately, there is a compelling line of evidence about CAPE from idealized simulations of tropical radiative-convective equilibrium (RCE) using higher-resolution cloud-resolving models (CRMs) that explicitly represent convective dynamics [Muller *et al.*, 2011; Romps, 2011; Singh and O'Gorman, 2013, 2014]. The CAPE increase seen in these CRM studies is roughly 8–12% per degree Celsius increase of sea surface temperature (SST), which agrees quantitatively with the results from GCMs. Most importantly, a theory for what processes set CAPE in RCE, and for how CAPE should change due to external forcings, was recently put forth by Singh and O'Gorman [2013, hereafter SO13].

The jumping-off point for the theory of SO13 is the observation that the actual buoyancies of tropical oceanic convective clouds are quite small—typically, less than 0.5 K when reported as condensate-loaded virtual temperature anomalies. This is true both in observations [e.g., Lawson, 1990; Wei *et al.*, 1998] and numerical

simulations of RCE [e.g., Sherwood *et al.*, 2013; Romps and Charn, 2015], and observed updraft velocities are correspondingly slow compared to what one would predict based on CAPE alone [Zipser and LeMone, 1980]. The smallness of cloud buoyancies indicates that the mean lapse rate of the tropical atmosphere is closely approximated by the lapse rate inside diluted convective clouds, a fact that motivated SO13 to consider the limit in which the buoyancy of an entraining bulk plume is exactly zero. This results in the attractively simple picture that an undilute parcel has finite CAPE because the clouds that set the temperature profile of the RCE state do not develop adiabatically, but instead strongly mix with air that is subsaturated. Gravity waves quickly flatten free-tropospheric temperatures in the tropics [Bretherton and Smolarkiewicz, 1989], giving the atmosphere an *entraining* lapse rate that is steeper than a moist adiabat. Since CAPE in this “zero-buoyancy” model results from the saturation deficit of air that entrains into clouds, SO13 argue that CAPE increases with warming because the saturation deficit is proportional to the saturation specific humidity, q_v^* , which scales with temperature according to the Clausius-Clapeyron (CC) relationship. This prediction of the zero-buoyancy theory was verified by the quasi-exponential increase in CAPE with SST seen in SO13’s cloud-resolving simulations of RCE.

The goal of this study is to rigorously determine whether undilute parcel buoyancy and CAPE scale with the saturation deficit of the troposphere. To do so, we implement two distinct methods of modifying the saturation deficit in a CRM: by varying the SST, as in SO13, and by varying the steady state environmental relative humidity (RH). In section 2, we use the zero-buoyancy model of SO13 to predict the atmosphere’s contrasting responses to these two forcings. In section 3, we find that when the SST is increased in the CRM, undilute buoyancy in the lower and middle troposphere does not increase because the CC scaling of the saturation deficit is balanced by a countervailing CC scaling of the factor that converts saturated moist static energy differences into temperature differences; we will refer to this conversion factor as β . In this warming experiment, undilute buoyancy can only increase with SST in the upper troposphere where β asymptotes to c_p , the heat capacity of dry air. However, in section 4, we find that increasing the saturation deficit by reducing the RH causes undilute buoyancy to increase throughout the troposphere because β does not change significantly as a function of RH. As shown in section 2, these two kinds of behavior are mathematically predicted by the equation for undilute buoyancy given by SO13.

2. CAPE in the Limit of Zero Buoyancy

The purpose of this section is to use a simple conceptual model to predict how the buoyancy of an adiabatic parcel should depend on the SST and environmental RH of an RCE state. This simple model necessarily neglects known features of cloud dynamics such as in-cloud heterogeneity [Jonas, 1990], stochastic mixing events [Romps and Kuang, 2010a], and buoyancy sorting [Taylor and Baker, 1991]; nevertheless, it will become clear that it retains significant predictive power.

We begin by giving an abbreviated derivation of the zero-buoyancy model of SO13. The basic idea of the zero-buoyancy model is to use the bulk plume moist static energy (MSE) budget to reason about $\Delta T_u = T_u - T$, where T_u is the temperature of an undilute parcel lifted from the surface and T is the environment temperature. In the limit of zero cloud buoyancy, T is given by the temperature of an entraining bulk plume. Since clouds are saturated at the environmental temperature in this limit, the MSE budget of the zero-buoyancy bulk plume is equivalent to a budget for the saturated MSE of the environment, h^* , and takes the particularly simple form

$$\partial_z h^* = -\epsilon (h^* - h) = -\epsilon L (1 - \text{RH}) q_v^*. \quad (1)$$

In equation (1), ϵ is the bulk plume fractional entrainment rate (units of m^{-1}), L is the latent heat of evaporation, h is the MSE of the environment, and the environmental subsaturation is determined by $\text{RH} \simeq q_v / q_v^*$, where q_v is the environmental specific humidity and q_v^* is the saturation specific humidity at the environmental temperature and pressure. For this simple model, the MSE is defined as $h = c_p T + gz + Lq_v$, with c_p being the heat capacity of dry air and g the gravitational acceleration; this definition of MSE contains the physics we need to build intuition for CAPE even though it ignores the ice phase and the effects of water on the heat capacity of moist air.

Equation (1) tells us that the entrainment of air with a saturation deficit of $(1 - \text{RH})q_v^*$ is what pushes the environment’s saturated MSE away from its value at the surface. Since an undilute parcel (approximately)

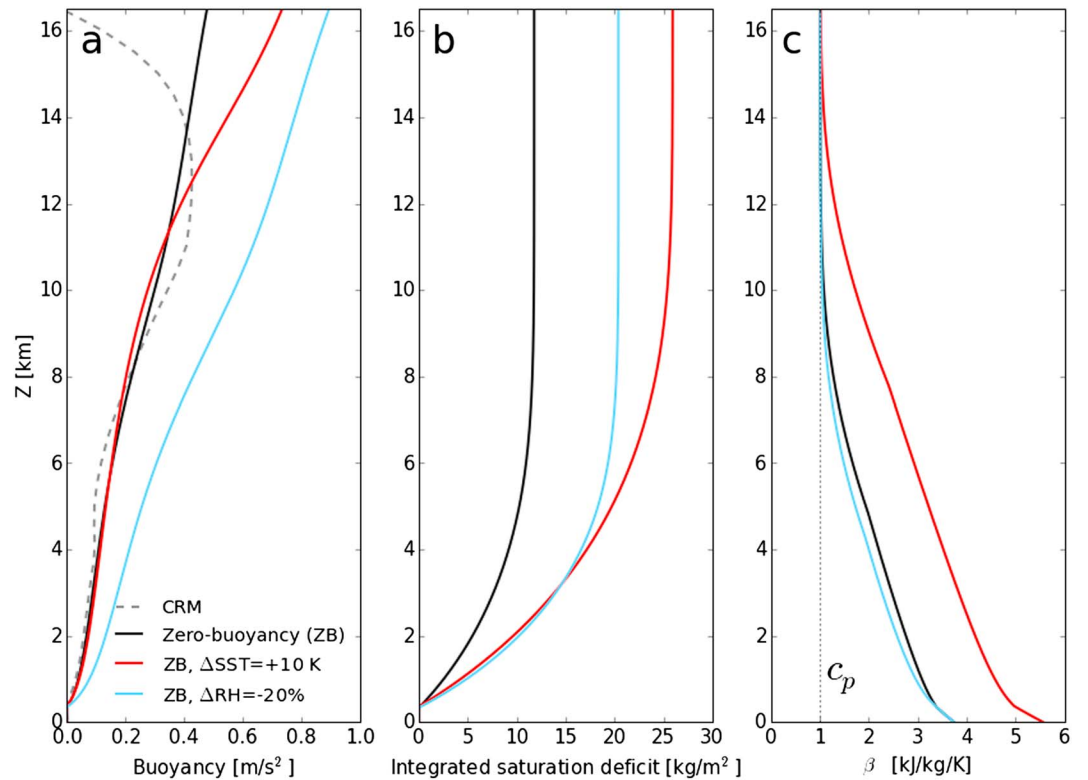


Figure 1. Profiles of (a) undilute near-surface parcel buoyancy, (b) vertically integrated saturation deficit $\int \rho(q_v^* - q_v) dz$, and (c) $\beta = c_p + L \frac{\partial q_v^*}{\partial T}$, as predicted by the simple version of the zero-buoyancy bulk plume model. Black lines correspond to a control case with an SST of 300 K and a free-tropospheric RH of 80%, while the red and blue lines are for a +10 K SST perturbation and a -20% RH perturbation, respectively. The zero-buoyancy model is run with a profile of bulk entrainment of the form $\epsilon(z) = 0.5/z$. Also plotted as a gray dashed line in Figure 1a is the profile of undilute buoyancy of an adiabatic parcel in a cloud-resolving simulation of RCE with an SST of 300 K.

conserves its MSE, equation (1) can be integrated vertically to find the saturated MSE surplus, Δh_u^* , of the undilute parcel at a given height z above the cloud base (which we take to be at z_0):

$$\Delta h_u^* = h_u^* - h^* = \int_{z_0}^z \epsilon L (1 - RH) q_v^* dz'. \quad (2)$$

To connect this to undilute buoyancy, we just need to convert Δh_u^* into ΔT_u by defining the function β , which satisfies $h^*(T + \Delta T) - h^*(T) = \beta \Delta T$. Linearizing q_v^* about T gives $\beta = c_p + L \frac{\partial q_v^*}{\partial T}$. This yields equation (4) from SO13:

$$\Delta T_u = \frac{1}{\beta} \int_{z_0}^z \epsilon L (1 - RH) q_v^* dz'. \quad (3)$$

Let us now consider how the zero-buoyancy model predicts ΔT_u should change as the SST is increased or as the RH is reduced. In Figure 1, we show results from a simple version of the zero-buoyancy plume model based on thermodynamics that are consistent with the equations given so far in section 2; for more details on the simple zero-buoyancy model, see section S1 in the supporting information. Figure 1a shows the undilute parcel buoyancy profiles predicted by the simple zero-buoyancy bulk plume model for a control case with SST = 300 K and RH = 80%, for an RH perturbation where free-tropospheric RH is reduced from 80% to 60%, and for an SST perturbation of +10 K. Both perturbations to the zero-buoyancy model increase the integrated saturation deficit by a similar amount in the lower troposphere, but they have starkly different effects on the buoyancy profile. Increasing the SST has essentially no effect on the profile of buoyancy below 11 km, while reducing the RH results in an approximate doubling of the buoyancy profile throughout the depth of the convecting layer. Why does the zero-buoyancy model act this way?

Figure 1c shows that it is the divergent effects of these two types of forcing on β that cause their effects on undilute buoyancy to differ so strongly. As an example, consider that both the SST perturbation and the RH

perturbation increase the vertically integrated saturation deficit at 5 km by roughly 80%, but the SST perturbation also increases β at this level by $\sim 80\%$, while the effect of the RH perturbation on β is an order of magnitude smaller.

Physically, the increase of β with temperature reflects the fact that a given Δh^* corresponds to a smaller ΔT in a warmer atmosphere because Δh^* is increasingly dominated by latent enthalpy (i.e., $L\Delta q_v$) rather than sensible heat (i.e., $c_p\Delta T$) as temperature increases. Generally, in layers of the atmosphere where β is dominated by the moist term given by $L\frac{\partial q_v^*}{\partial T}$, equation (3) suggests that ΔT_u should be insensitive to increasing temperature because both the integrated saturation deficit and β exhibit CC scaling. This should be the case for typical lower troposphere tropical conditions in the current climate (e.g., at a temperature of 300 K and a pressure of 1000 mbar, roughly 75% of β comes from the moist term).

However, assuming that convection always extends at least to an altitude with a typical anvil temperature of ~ 220 K [Hartmann and Larson, 2002], there is a layer of the upper atmosphere where q_v^* is small enough that β asymptotes to c_p . Even though q_v^* is small in the upper troposphere, the vertically integrated saturation deficit is not small because it includes the saturation deficit in lower, warmer layers of the atmosphere; therefore, where $\beta \simeq c_p$, the increase of the saturation deficit that accompanies a warming atmosphere can efficiently cause increases in undilute buoyancy. This is reflected in Figure 1, where the SST perturbation does increase undilute buoyancy at altitudes above 11 km.

In this section, we have shown that the zero-buoyancy model of SO13 predicts undilute parcel buoyancy in the lower and middle troposphere to be relatively insensitive to an SST warming perturbation, but to increase with SST in the upper troposphere. In contrast, we have also shown that the zero-buoyancy model predicts undilute buoyancy throughout the troposphere to be quite sensitive to an RH reduction perturbation (Figure 1). These differences suggest that while modulating the saturation deficit does change CAPE in the zero-buoyancy framework, exactly how the saturation deficit is changed matters very much for how the vertical profile of undilute buoyancy responds. In the remaining sections of the paper, we present the results from a CRM that is subjected to an SST warming experiment and an RH-varying experiment to test the conclusions drawn from the simple framework presented thus far.

3. SST Warming Experiment

All cloud-resolving simulations in this work were performed with Das Atmosphärische Modell [Romps, 2008]. For this experiment, simulations were run on a square, doubly periodic domain with a model top at 61 km and a vertical grid spacing that varies smoothly from 50 m in the boundary layer to 500 m at a height of 5 km and to 1 km at 50 km. The lower boundary was specified to be an ocean surface with a fixed SST of 290, 300, 310, or 320 K. Surface fluxes were calculated using a bulk formula, and shortwave and longwave radiation were calculated interactively; there is no ozone in these simulations, and the same vertically constant 280 ppmv CO₂ profile was used for all simulations. Each of the four SST cases was first run to RCE over the course of approximately 400 days on a small domain (32 km width) with 2 km horizontal resolution, after which the simulations were restarted on a larger 72 km domain with 500 m horizontal resolution. The higher-resolution, larger-domain simulations were run for an additional 60 days, with statistics collected over the last 30 days of equilibrated convection. Horizontal- and time-mean vertical profiles of quantities of interest were recorded, as well as mean profiles within “cloud updrafts”; cloud updrafts were identified as grid cells with nonprecipitating condensed water mass fraction greater than 10^{-5} and vertical velocity greater than 1 m/s.

Figure 2a shows the buoyancy profiles of adiabatically lifted air parcels (assuming no condensate fallout) in the four simulations of RCE over SSTs of 290, 300, 310, and 320 K. Parcels were initialized with the mean temperature, pressure, and moisture content of the near-surface CRM level, and their buoyancies were calculated by lifting through the horizontal- and time-mean environmental density profile assuming conservation of MSE-CAPE [Romps, 2015] with a full treatment of the thermodynamics of water, including the ice phase.

The undilute buoyancy profiles in Figure 2a from the four CRM simulations collapse onto a common curve below ~ 8 km, but as the SST is raised, the profiles develop an increasingly prominent peak in the upper troposphere. On these profiles, circles indicate the point where β transitions from being mostly moist ($L\frac{\partial q_v^*}{\partial T} > c_p$) to mostly dry ($L\frac{\partial q_v^*}{\partial T} < c_p$). This point serves as an approximate division between the two regimes discussed in section 2: where β is dominated by the moist term, the zero-buoyancy model predicts that undilute buoyancy should be fairly insensitive to increasing SST because ΔT_u is given by the ratio of two quantities that both

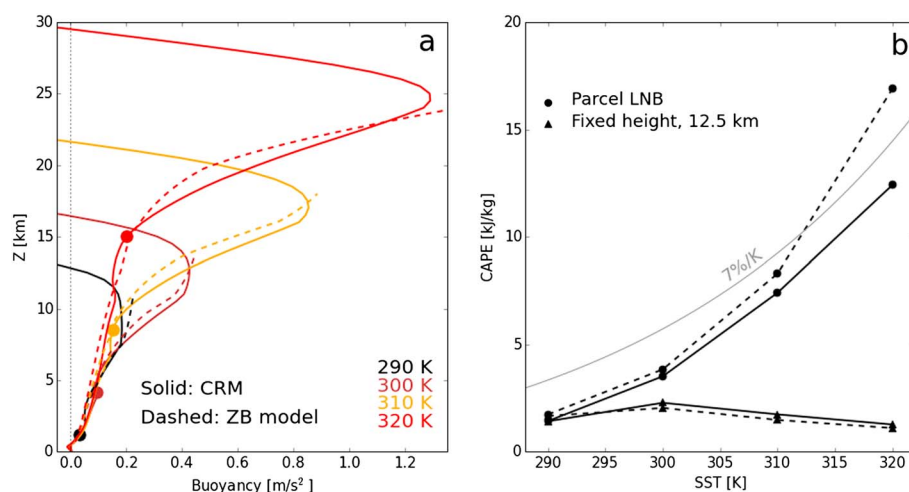


Figure 2. (a) Profiles of buoyancy for adiabatically lifted near-surface air parcels for SSTs of 290 K (black), 300 K (brown), 310 K (orange), and 320 K (red). Solid lines correspond to CRM simulations of RCE, while the predictions of the complex zero-buoyancy model are plotted in dashed lines up to a temperature of 200 K. Colored circles indicate the point on the buoyancy profile above which β is dominated by c_p rather than $L \frac{\partial q_s^*}{\partial T}$. The zero-buoyancy model is run with a profile of bulk entrainment of the form $\epsilon(z) = 0.8/z$. (b) CAPE as a function of SST when integrated up to the undilute parcel LNB (circles) or to a fixed altitude of 12.5 km (triangles). As in Figure 2a, solid lines are results from the CRM and dashed lines are from the zero-buoyancy model.

exhibit Clausius-Clapeyron scaling; conversely, where β is dominated by the dry term, we expect the increase in the integrated saturation deficit with atmospheric warming to be fully expressed as larger undilute parcel buoyancy. Figure 2a shows that this moist-to-dry transition of β , which occurs at a higher altitude in warmer atmospheres, identifies the point in each profile where undilute parcel buoyancy rapidly increases.

These high buoyancies in the upper troposphere define a reservoir of CAPE between the β transition point and the undilute parcel LNB that accounts for between 85% and 99% of the total CAPE in our CRM simulations. Since the undilute buoyancies in this layer of the atmosphere are (by definition) in a regime where increases in the saturation deficit are efficiently expressed as larger undilute parcel temperature excesses, and since these buoyancies dominate CAPE, the SST scaling of CAPE should bear the imprint of the Clausius-Clapeyron scaling of the saturation deficit. Figure 2b plots CAPE as a function of SST when integrated up to the undilute parcel's level of neutral buoyancy (LNB). This CAPE increases quasi-exponentially with a best fit rate of $\sim 7\%/K$ over the simulated 30 K range. We also show CAPE integrated up to a fixed height of 12.5 km, which is the highest level at which all simulations have positively buoyant undilute parcels; for this fixed upper bound, the CAPE change with SST is flat and nonmonotonic because the layers of the atmosphere where undilute buoyancy can respond to the increase in the saturation deficit are excluded. Assuming a pseudoadiabatic lifting process with complete condensate fallout slightly softens the contrast between buoyancy behavior in the lower and upper troposphere but does not modify these conclusions. (For a pseudoadiabatic parcel, the increase of the virtual effect in the lower troposphere with SST is not balanced by an increase in condensate loading, and total buoyancy in the lower troposphere increases slightly even though the absolute temperature anomaly of the parcels remains insensitive to SST; see Figure 2a of SO13 for pseudoadiabatic virtual temperature anomalies over a colder range of SSTs.)

Figure 2a also shows the undilute parcel buoyancy profiles predicted by the zero-buoyancy model for the four SSTs we simulated with the CRM. For completeness, here we use a complex version of the zero-buoyancy plume model that is formulated with thermodynamics that includes the full effects of water on the density and heat capacity of moist air; for more details on the complex zero-buoyancy model, see section S2. The match between the zero-buoyancy model and the CRM results is striking. The zero-buoyancy model captures both the insensitivity of undilute buoyancy to SST below ~ 8 km as well as (in the warmer simulations with larger saturation deficits) the rapid increase in buoyancy with altitude in the regime where β is predominantly dry. Figure 2b shows that CAPE predicted by the zero-buoyancy model also increases rapidly as a function of SST when integrated up to the CRM-diagnosed undilute parcel LNB (in fact, it overestimates the CAPE increase in

this case, because it misses the decrease of parcel buoyancy toward zero as the LNB is approached). On the other hand, when integrated up to a fixed height of 12.5 km, the zero-buoyancy CAPE as a function of SST is flat.

4. RH-Varying Experiment

For this experiment, we change the mean relative humidity of air that mixes with developing clouds in the RCE state of our CRM by manipulating the water budget outside of clouds. In convecting regions of the real tropical troposphere, relative humidities hover around 80%, with a characteristic “C” shape that has a minimum around 7 km. In fact, by generalizing the zero-buoyancy model of SO13 to incorporate detrainment of saturated air from clouds, Romps [2014] showed that this shape of tropical relative humidity results from how the strengths of two competing effects of convection—moistening by detrainment and drying by forced subsidence—typically vary with altitude. In a CRM, however, we can force the atmosphere away from its natural profile of relative humidity, isolating and manipulating the effect of environmental humidity on the lapse rate and undilute buoyancy.

There is a deep literature regarding the sensitivity of convection to the humidity of the environment in which it develops, but our experiment is novel mainly because it considers steady state convection. It is a commonplace observation that dry air at midlevels reduces cloud buoyancies by entrainment, effectively suppressing deep convection and reducing precipitation [e.g., Mapes and Zuidema, 1996; Brown and Zhang, 1997; Parsons *et al.*, 2000; Derbyshire *et al.*, 2004; Takemi *et al.*, 2004]. The importance of deep convective “preconditioning”—that is, the gradual erosion of a dry inhibition layer by progressively deeper cumulus development—has also been demonstrated in numerical simulations of tropical convection [Kuang and Bretherton, 2006], the diurnal cycle over land [Chaboureau *et al.*, 2004], and many other scenarios [e.g., Ridout, 2002; Khairoutdinov and Randall, 2006; Waite and Khouider, 2010]. However, these prior simulations are transient in the sense that initial profiles of environmental humidity are allowed to evolve under the influence of convection. We are interested in the steady state behavior—what if we don’t allow shallow convection to pave the way for the clouds that make it all the way to the tropopause?

Our cloud-resolving simulations for this experiment were conducted on a 30^3 km³ domain with doubly periodic horizontal boundaries. All simulations used the same vertical grid with 50 m spacing below 600 m altitude, increasing continuously to a constant 100 m spacing between 1 and 15 km altitude and then increasing again to 1 km spacing in the stratosphere. (This relatively high vertical resolution throughout the troposphere is required to maintain numerical stability at high relative humidities.)

The atmosphere in this experiment was destabilized by a fixed (noninteractive) radiative cooling profile of 1.5 K/d from the surface up to an altitude of 10 km, decreasing to 0 K/d linearly in altitude between 10 and 15 km. The use of noninteractive radiative cooling essentially fixes the depth of the convective layer. We first ran a control simulation to RCE over an SST of 300 K with 2 km horizontal resolution. We saved the mean vertical temperature profile from the equilibrated phase of this control run, and our forced-RH simulations were then branched from a 3-D snapshot of the model state at the end of the control and run to RCE. The model state at the end of these 2 km resolution runs for each target RH value was then interpolated to a grid with 500 m horizontal grid spacing and continued. After the simulations adjusted to the new resolution, statistics were collected over 10 days of equilibrated convection. As in the SST warming experiment presented in section 3, we recorded domain-mean vertical profiles of quantities of interest as well as mean profiles within “cloud updrafts” identified by thresholds for condensed water content and vertical velocity.

A schematic of the forcings employed in our forced-RH experiments is shown in Figure 3a. The setup should be thought of in terms of three layers: a subcloud-layer thermodynamic “sponge” whose purpose is to maintain constant moist entropy, a free troposphere that is destabilized by radiation and nudged toward a particular value of relative humidity in the clear-sky regions, and a stratospheric sponge that absorbs overshooting convection. In the stratosphere ($z > 15$ km), the only thermodynamical forcing is a nudging of layer mean temperatures to their values from the control simulation on a timescale of 6 h. In the subcloud layer ($z < 400$ m), temperatures were nudged locally (i.e., grid point by grid point) to the mean value at that elevation from the control simulation on a timescale of 1 min. We use local temperature nudging, rather than nudging of the mean, because nudging layer mean temperatures is problematic when there is an excessively large variance in low-level thermodynamical properties, as there is in simulations with very strong cold pools (the drier simulations).

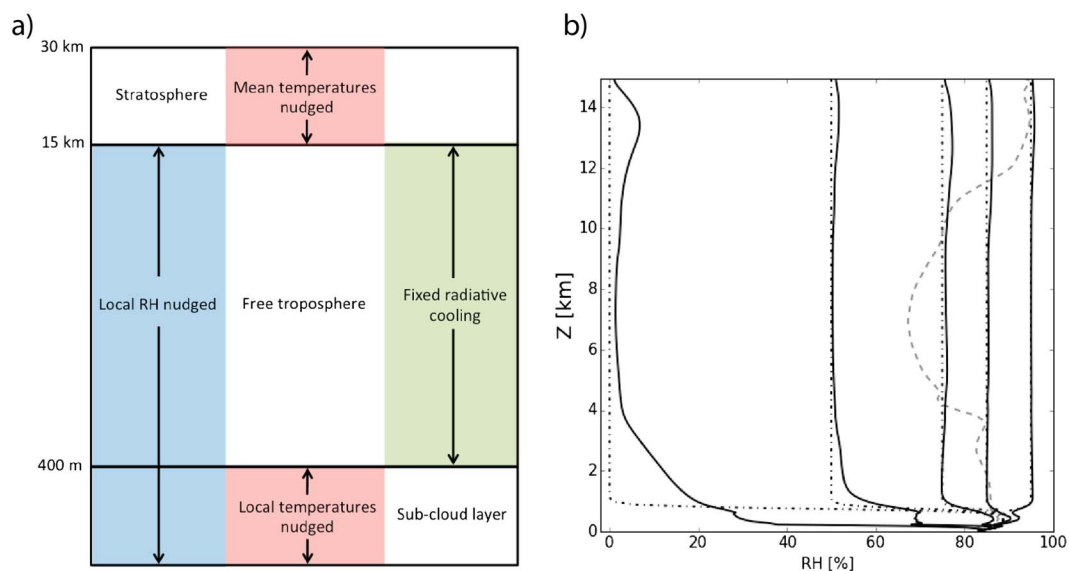


Figure 3. (a) A schematic of the forcings employed in the RH-varying experiment of section 4. In the stratosphere ($z > 15$ km), layer mean temperatures are nudged to their values from a control simulation. In the free troposphere ($400 \text{ m} \leq z \leq 15$ km), a fixed radiative cooling profile is applied and the relative humidity outside of clouds is nudged toward a target value. In the subcloud layer ($z < 400$ m), relative humidity is also nudged, and temperature is nudged grid point by grid point toward the mean value at that altitude from a control simulation. (b) Steady state RH profiles from our simulations (solid lines), corresponding to forcing profiles with free-tropospheric values of 0%, 50%, 75%, 85%, and 95%. The forcing profiles are indicated by the dash-dotted lines. For reference, the relative humidity profile of an unforced RCE simulation is also shown by a gray dashed line.

Figure 3b shows the relative humidity forcings, which were specified by a series of smoothly varying target RH profiles, $\text{RH}^\dagger(z)$, corresponding to free-tropospheric target values in the set $\{0\%, 50\%, 75\%, 85\%, 95\%\}$. Each profile has the same shape below 400 m, with values of roughly 85% as are observed below cloud base in standard RCE, before transitioning to the varying free-tropospheric values between 500 m and 1 km. We implement the RH forcing by nudging unsaturated grid points toward the target RH value via a mole-for-mole swap of dry air and water vapor that is enforced by source terms in the governing equations for water vapor and dry air. The forcing operates on an altitude-dependent timescale that is chosen to be short in the subcloud-layer, long in the neighborhood of cloud base (so that clouds have a chance to become saturated), and short again in the free troposphere; for more details of the relative humidity forcing framework, see section S3. Figure 3b shows the resulting steady state environmental relative humidity profiles in our simulations.

The buoyancy profiles of adiabatically lifted air parcels for the five simulations of RCE corresponding to target free-tropospheric RH values of 0%, 50%, 75%, 85%, and 95% are shown in Figure 4a. The buoyancy profiles in this experiment tell a very different story than those from the SST warming experiment shown in Figure 2a. The undilute parcel LNB remains fixed at ~ 15 km, while the buoyancy at all heights between cloud base and the LNB increases monotonically with decreasing environmental RH. This confirms, over a much wider range of RH values, the prediction of the simple zero-buoyancy model in section 2 that undilute parcel buoyancy throughout the troposphere is very sensitive to the RH of air that entrains into clouds. Unlike in the SST warming experiment, where the increase of β with SST caused the altitude of the β moist-to-dry transition point to increase from roughly 1 km to 15 km, β decreases weakly with decreasing RH, and the β transition point only shifts from 5 km down to 2.5 km. This relative insensitivity of β allows increases in the saturation deficit to be straightforwardly expressed as increases in undilute buoyancy throughout the troposphere in the RH-varying experiment.

Also plotted in Figure 4a are the undilute buoyancy profiles predicted by the complex-thermodynamics version of the zero-buoyancy model. The zero-buoyancy model is run with the same fixed entrainment rate profile as in the SST warming experiment but supplied with the varying RH profiles from the CRM (i.e., the steady

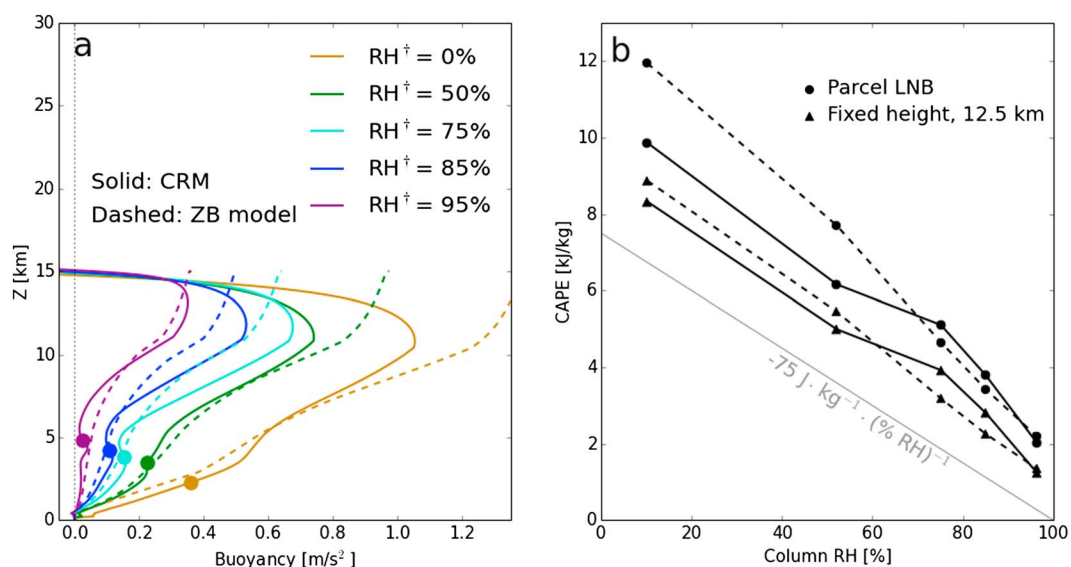


Figure 4. As in Figure 2 but for the RH-varying experiment. (a, b) Solid lines are results from the CRM, and dashed lines are from the zero-buoyancy model. The zero-buoyancy model is supplied with the same entrainment rate profile as in Figure 2 and with the corresponding relative humidity profile from Figure 3b. In Figure 4a, colors correspond to the range of target free-tropospheric relative humidities and colored circles mark where β transitions from being mostly moist to mostly dry. In Figure 4b, CAPE is integrated up to either the undilute parcel LNB (circles) or to a fixed altitude of 12.5 km (triangles).

state profiles shown in Figure 3b). The zero-buoyancy model's match with the CRM results is excellent, capturing both the shape and magnitude of the increase in undilute buoyancy with decreasing RH seen in the CRM results. When integrated up to the undilute parcel LNB or to a fixed height of 12.5 km, CAPE in the CRM and zero-buoyancy model both decrease strongly with increasing column RH (Figure 4b), with a sensitivity of approximately $-75 \text{ J/kg}/(\% \text{ RH})$.

5. Conclusions

The fact that the zero-buoyancy model of SO13 can explain the CAPE variations in a convecting atmosphere subjected to two drastically different types of forcing—increases in SST and decreases in environmental RH—implies that it captures the fundamental physics of CAPE. Building on the work of SO13, we have shown that CAPE exhibits Clausius-Clapeyron scaling because undilute buoyancies in the upper troposphere dominate CAPE and scale with the vertically integrated saturation deficit. This adds specificity to the widely repeated claim that warming temperatures increase the “amount of fuel” available for deep convection—our work shows that while increases in q_v^* do increase the difference in saturated MSE (Δh_u^*) between an undilute parcel and its environment, the larger Δh_u^* is only expressed as larger buoyancy in layers of the troposphere where the scarcity of water vapor forces Δh_u^* to be dominated by sensible heat rather than latent enthalpy.

As a final note, we point out that there is no a priori connection between changes in the buoyancy of fictional adiabatic parcels and changes in actual updraft speeds, because the clouds in CRM simulations and in the real tropical atmosphere are highly diluted [Romps and Kuang, 2010b; Fierro et al., 2009]. However, Figure S1 shows that the mean vertical velocity of the cloud updrafts in our two experiments changes in the same sense as the undilute buoyancies: for the SST warming experiment, the velocities collapse onto a common curve that increases with altitude and grows taller with SST, while for the RH-varying experiment, the updraft speeds increase dramatically at all altitudes in the convective layer as RH is lowered. The connection between warming SSTs, entrainment, and the vertical velocity of the most intense (i.e., most weakly entraining) updrafts was explored through the generalized two-plume zero-buoyancy model of Singh and O’Gorman [2014], but it remains unclear why the mean vertical velocity of highly diluted clouds should change in the same manner as undilute buoyancy. Whether this is a coincidence or physically constrained is a fascinating and difficult question that we leave to future work.

Acknowledgments

J.S. thanks J. Edman, N. Jeevanjee, W. Langhans, and D. Yang for their thoughtful questions and suggestions. The authors are grateful for two anonymous reviewers whose feedback improved the manuscript. J. S. was supported by the National Science Foundation Graduate Research Fellowship under grant DGE1106400. D.R. was supported by the Scientific Discovery through Advanced Computing (SciDAC) program funded by U.S. Department of Energy Office of Advanced Scientific Computing Research and Office of Biological and Environmental Research under contract DE-AC02-05CH11231. This research used computing resources of the National Energy Research Scientific Computing Center (NERSC), which is supported by the Office of Science of the U.S. Department of Energy under contract DE-AC02-05CH11231.

References

- Bretherton, C. S., and P. K. Smolarkiewicz (1989), Gravity waves, compensating subsidence, and detrainment around cumulus clouds, *J. Atmos. Sci.*, *46*(4), 740–759.
- Brooks, H. (1994), On the environments of tornadic and nontornadic mesocyclones, *Weather and Forecasting*, *9*, 606–618.
- Brown, R. G., and C. Zhang (1997), Variability of midtropospheric moisture and its effect on cloud-top height distribution during TOGA COARE*, *J. Atmos. Sci.*, *54*(23), 2760–2774, doi:10.1175/1520-0469(1997)054<2760:VOMMAI>2.0.CO;2.
- Chaboureaud, J. Å., F. Guichard, J. Å. Redelsperger, and J. Å. Lafore (2004), The role of stability and moisture in the diurnal cycle of convection over land, *Q. J. R. Meteorol. Soc.*, *130*(604), 3105–3117, doi:10.1256/qj.03.132.
- Derbyshire, S., I. Beau, P. Bechtold, J.-Y. Grandpeix, J.-M. Piriou, J.-L. Redelsperger, and P. Soares (2004), Sensitivity of moist convection to environmental humidity, *Q. J. R. Meteorol. Soc.*, *130*(604), 3055–3079, doi:10.1256/qj.03.130.
- Diffenbaugh, N. S., M. Scherer, and R. J. Trapp (2013), Robust increases in severe thunderstorm environments in response to greenhouse forcing, *Proc. Natl. Acad. Sci. U.S.A.*, *110*(41), 16,361–16,366, doi:10.1073/pnas.1307758110.
- Fasullo, J. (2011), A mechanism for land-ocean contrasts in global monsoon trends in a warming climate, *Clim. Dyn.*, *39*(5), 1137–1147, doi:10.1007/s00382-011-1270-3.
- Fierro, A. O., J. Simpson, M. A. LeMone, J. M. Straka, and B. F. Smull (2009), On how hot towers fuel the Hadley cell: An observational and modeling study of line-organized convection in the equatorial trough from TOGA COARE, *J. Atmos. Sci.*, *66*(9), 2730–2746, doi:10.1175/2009JAS3017.1.
- Hartmann, D., and K. Larson (2002), An important constraint on tropical cloud-climate feedback, *Geophys. Res. Lett.*, *29*(20), 1951, doi:10.1029/2002GL015835.
- Jonas, P. R. (1990), Observations of cumulus cloud entrainment, *Atmos. Res.*, *25*, 105–127, doi:10.1016/0169-8095(90)90008-Z.
- Khairoutdinov, M., and D. Randall (2006), High-resolution simulation of shallow-to-deep convection transition over land, *J. Atmos. Sci.*, *63*(12), 3421–3436, doi:10.1175/JAS3810.1.
- Kuang, Z., and C. S. Bretherton (2006), A mass-flux scheme view of a high-resolution simulation of a transition from shallow to deep cumulus convection, *J. Atmos. Sci.*, *63*, 1895–1909.
- Lawson, R. P. (1990), Performance of some airborne thermometers in clouds, *J. Atmos. Oceanic Technol.*, *7*, 480–494, doi:10.1175/1520-0426(1990)007<0480:POSATI>0.CO;2.
- Lepore, C., D. Veneziano, and A. Molini (2014), Temperature and CAPE dependence of rainfall extremes in the eastern United States, *Geophys. Res. Lett.*, *42*, 74–83, doi:10.1002/2014GL062247.
- Lin, J.-L., T. Qian, T. Shinoda, and S. Li (2015), Is the tropical atmosphere in convective quasi-equilibrium?, *J. Clim.*, *28*, 4357–4372, doi:10.1175/JCLI-D-14-00681.1.
- Mapes, B. E., and P. Zuidema (1996), Radiative-dynamical consequences of dry tongues in the tropical troposphere, *J. Atmos. Sci.*, *53*, 620–638, doi:10.1175/1520-0469(1996)053<0620:RDCODT>2.0.CO;2.
- Muller, C. J., P. A. O’Gorman, and L. E. Back (2011), Intensification of precipitation extremes with warming in a cloud-resolving model, *J. Clim.*, *24*(11), 2784–2800, doi:10.1175/2011JCLI3876.1.
- Parsons, D. B., K. Yoneyama, and J.-L. Redelsperger (2000), The evolution of the atmosphere-ocean systems over the tropical western Pacific following the arrival of a dry intrusion, *Q. J. R. Meteorol. Soc.*, *126*, 517–548.
- Ridout, J. A. (2002), Sensitivity of tropical Pacific convection to dry layers at mid- to upper levels: Simulation and parameterization tests, *J. Atmos. Sci.*, *59*(23), 3362–3381, doi:10.1175/1520-0469(2002)059<3362:SOTPCT>2.0.CO;2.
- Romps, D. M. (2008), The dry-entropy budget of a moist atmosphere, *J. Atmos. Sci.*, *65*(12), 3779–3799, doi:10.1175/2008JAS2679.1.
- Romps, D. M. (2011), Response of tropical precipitation to global warming, *J. Atmos. Sci.*, *68*(1), 123–138, doi:10.1175/2010JAS3542.1.
- Romps, D. M. (2014), An analytical model for tropical relative humidity, *J. Clim.*, *27*(19), 7432–7449, doi:10.1175/JCLI-D-14-00255.1.
- Romps, D. M. (2015), MSE minus CAPE is the true conserved variable for an adiabatically lifted parcel, *J. Atmos. Sci.*, *72*, 3639–3646.
- Romps, D. M., and A. B. Charn (2015), Sticky thermals: Evidence for a dominant balance between buoyancy and drag in cloud updrafts, *J. Atmos. Sci.*, *72*, 2890–2901.
- Romps, D. M., and Z. Kuang (2010a), Nature versus nurture in shallow convection, *J. Atmos. Sci.*, *67*(5), 1655–1666, doi:10.1175/2009JAS3307.1.
- Romps, D. M., and Z. Kuang (2010b), Do undiluted convective plumes exist in the upper tropical troposphere?, *J. Atmos. Sci.*, *67*(2), 468–484, doi:10.1175/2009JAS3184.1.
- Romps, D. M., J. T. Seeley, D. Vollaro, and J. Molinari (2014), Projected increase in lightning strikes in the United States due to global warming, *Science*, *346*(6211), 851–854, doi:10.1126/science.1259100.
- Seeley, J. T., and D. M. Romps (2015), The effect of global warming on severe thunderstorms in the United States, *J. Clim.*, *28*, 2443–2458, doi:10.1175/JCLI-D-14-00382.1.
- Sherwood, S. C., D. Hernández-Deckers, M. Colin, and F. Robinson (2013), Slippery thermals and the cumulus entrainment paradox*, *J. Atmos. Sci.*, *70*(8), 2426–2442, doi:10.1175/JAS-D-12-0220.1.
- Singh, M. S., and P. A. O’Gorman (2013), Influence of entrainment on the thermal stratification in simulations of radiative-convective equilibrium, *Geophys. Res. Lett.*, *40*, 4398–4403, doi:10.1002/grl.50796.
- Singh, M. S., and P. A. O’Gorman (2014), Increase in moist-convective updraft velocities with warming in radiative-convective equilibrium, *Q. J. R. Meteorol. Soc.*, *17*, 1–12.
- Sobel, A. H., and S. J. Camargo (2011), Projected future seasonal changes in tropical summer climate, *J. Clim.*, *24*(2), 473–487, doi:10.1175/2010JCLI3748.1.
- Takemi, T., O. Hirayama, and C. Liu (2004), Factors responsible for the vertical development of tropical oceanic cumulus convection, *Geophys. Res. Lett.*, *31*, L11109, doi:10.1029/2004GL020225.
- Taylor, G., and M. Baker (1991), Entrainment and detrainment in cumulus clouds, *J. Atmos. Sci.*, *48*(1), 112–121.
- Waite, M. L., and B. Khouider (2010), The deepening of tropical convection by congestus preconditioning, *J. Atmos. Sci.*, *67*(8), 2601–2615, doi:10.1175/2010JAS3357.1.
- Wei, D., A. M. Blyth, and D. J. Raymond (1998), Buoyancy of convective clouds in TOGA COARE, *J. Atmos. Sci.*, *55*(22), 3381–3391, doi:10.1175/1520-0469(1998)055<3381:BOCCIT>2.0.CO;2.
- Williams, E. R., S. Rutledge, S. Geotis, N. Renno, E. Rasmussen, and T. Rickenbach (1992), A radar and electrical study of tropical “hot towers”, *J. Atmos. Sci.*, *49*(15), 1386–1395.
- Zipser, E., and M. LeMone (1980), Cumulonimbus vertical velocity events in GATE. Part II: Synthesis and model core structure, *J. Atmos. Sci.*, *37*, 2458–2469.

Supporting Information for “Why does tropical convective available potential energy (CAPE) increase with warming?”

Jacob T. Seeley^{1,2} and David M. Romps^{1,2}

Contents of this file

1. Text S1 to S3
2. Figure S1

Corresponding author: J. T. Seeley, Department of Earth and Planetary Science, University of California, Berkeley, 449 McCone Hall, Berkeley, CA 94703, USA. (jseeley@berkeley.edu)

¹Department of Earth and Planetary Science, University of California, Berkeley, California, USA.

²Climate and Ecosystem Sciences Division, Lawrence Berkeley National Laboratory, Berkeley, California, USA.

Text S1: Simple zero-buoyancy model

The simple zero-buoyancy model is based on a simplified thermodynamics in which there is no ice phase. In addition, the effect of water on the density and heat capacity of air is neglected. Accordingly, MSE is defined here as $h = c_p T + Lq_v + gz$. The plume equations describing the vertical profiles of saturated MSE h^* , total water ($q_t = q_v + q_c$, where q_c is the non-precipitating condensed water), and pressure are:

$$\partial_z h^* = -\epsilon (h^* - h) , \quad (1)$$

$$\partial_z q_t = -\epsilon (q_t - q_v) , \quad (2)$$

$$\partial_z \log p = -g/(R_a T) . \quad (3)$$

The MSE of the environment is given by h , q_v is the specific humidity of the environment, and R_a is the dry-air gas constant. The plume equations are integrated vertically by first specifying the temperature, total water, and pressure at plume base. If the plume is initially unsaturated, as it typically is when initialized with values taken from the near-surface level of a CRM simulation, equations 1–3 are advanced with the entrainment rate ϵ set to 0 to generate a dry adiabat until saturation occurs. At and above the level of plume saturation, the specific humidity and the MSE of the environment are calculated using the supplied RH profile and the known temperature of the plume/environment. The supplied entrainment profile is then used to calculate the plume's q_t and h^* at the next vertical step with a simple forward-difference method. A root-solver is used to calculate the temperature that is consistent with the known value of h^* at the next vertical step. Any water in excess of q_v^* is dumped into the q_c category. As it is written, equation 2 assumes no fallout of condensed water, but our plume model includes a parameter, γ , that determines

what fraction of liquid water precipitates out at each step. If $1 \geq \gamma > 0$, any new q_c that forms when stepping vertically is reduced by the factor $(1 - \gamma)$. This “precipitation” is removed at constant pressure and temperature. Since we neglect the effect of water on the density and pressure of air in this simple model, q_c only functions as a reserve of liquid water that can re-evaporate to maintain saturation after entrainment reduces the specific humidity of the plume. Iterating this procedure generates a plume/environment temperature profile. The buoyancy of an undilute parcel is then computed by lifting a parcel that conserves its (simple) MSE, computing its temperature as a function of height, and comparing to the plume/environment temperature profile. Note that the zero-buoyancy plume is always colder than the undilute parcel—the zero-buoyancy model does not predict an LNB. To get a value of CAPE from the buoyancy profile predicted by the zero-buoyancy model, one must supply an upper bound for the CAPE integration. The plume models are implemented in Python; code is available from the first author upon request.

Text S2: Complex zero-buoyancy model

Like the simple version, the complex zero-buoyancy model operates on the principle of neutrality between an entraining plume and its environment, but takes full account of the ice phase and the effects of water on the density and heat capacity of air. The total water mass fraction in this case is $q_t = q_v + q_l + q_s$, where q_l and q_s are the mass fractions of liquid and solid water, respectively. The MSE is given by

$$h = c_{pm}(T - T_0) + q_v(E_{0v} + R_v T_0) - q_s E_{0s} + gz, \quad (4)$$

where c_{pm} is the constant-pressure specific heat capacity of moist air, $T_0 = 273.16$ K is the triple-point temperature, E_{0v} is the difference in specific internal energy between water vapor and liquid at the triple-point temperature, R_v is the gas constant for water vapor, and E_{0s} is the difference in specific internal energy between water liquid and solid at the triple-point temperature. The moist-air heat capacity, c_{pm} , is given as a mass-fraction-weighted linear combination of the constant-pressure heat capacities of dry air (subscript a) and the three water phases (subscripts v , l , and s): $c_{pm} = q_a c_{pa} + q_v c_{pv} + q_l c_{pl} + q_s c_{ps}$.

The complex version of the zero-buoyancy model integrates the same plume equations as the simple version, but the pressure equation is replaced with

$$\partial_z \log p = \frac{-g}{R_m T_e}, \quad (5)$$

where $R_m = q_v R_v + (1 - q_v) R_d$ is the gas constant for moist environmental air and T_e is the environment temperature. The vertical integration of the plume equations is carried out as for the simple model, but since we include the effects of water phases on the density of air in this case, the neutrality of the entraining plume is enforced as a constraint on density rather than temperature. A rootsolving algorithm uses the known plume density and the supplied environmental relative humidity to calculate the environmental temperature that is consistent with a neutrally buoyant plume. The complex version of the zero-buoyancy model also includes the full effects of the ice phase; q_v^* is defined with respect to liquid at temperatures warmer than the triple-point temperature (273.16 K), with respect to ice at temperatures below 240 K, and as a linear combination of the two at temperatures in between. This corresponds to a non-isothermal mixed phase regime between the triple-point temperature and the temperature of homogeneous freezing; the

partitioning of condensates in the plume transitions linearly in temperature from all-liquid to all-ice between these two temperatures. (For a more complete description of the moist thermodynamics used in this model, including explicit equations for q_v^* , see the appendix of *Romps (2015)*). To calculate undilute parcel buoyancy, a near-surface parcel is lifted assuming conservation of MSE - CAPE, and this parcel’s density is then compared to the plume/environment density profile produced by the zero-buoyancy model. The plume models are implemented in Python; code is available from the first author upon request.

Text S3: Method for nudging RH

There are many ways one could “nudge” relative humidity in a numerical model, so here we will be explicit about how this forcing was implemented in our simulations. Our relative humidity nudging was performed by nudging the local q_v according to

$$F_{q_v} = \rho \frac{\text{RH}^\dagger(z)q_v^* - q_v}{\tau}, \quad (6)$$

where $\text{RH}^\dagger(z)$ is the target RH profile and the nudging timescale is τ . Note that F_{q_v} has units of density per time, and represents an artificial convergence of pure water vapor into the Eulerian finite volumes in the numerical model (we use “convergence” as shorthand for convergence or divergence). That is, F_{q_v} appears as a source in the governing equation for water vapor as follows:

$$\partial_t (q_v \rho) = -\vec{\nabla} \cdot (q_v \rho \vec{u}) + e - \vec{\nabla} \cdot \vec{d}_v + F_{q_v}, \quad (7)$$

where the other source terms are the resolved-flow moisture convergence $-\vec{\nabla} \cdot (q_v \rho \vec{u})$, the evaporation e , and the convergence of diffusive vapor fluxes $-\vec{\nabla} \cdot \vec{d}_v$, which is nonzero only in the near-surface level in our model.

However, since we are interested in the effect of environmental relative humidity on the temperature profile of a convecting atmosphere, we need to adjust RH in such a way that the forcing itself has negligible effects on temperature. The convergence of water vapor does work on the gas in a finite volume, and therefore has an effect on temperature. To counteract this, we also specify a countervailing convergence of an equal and opposite number of moles of dry air per volume per time:

$$F_{q_a}(z) = -\frac{R_v}{R_a}F_{q_v}. \quad (8)$$

The end result of this combination of forcings is effectively a mole-for-mole swap of dry air and water vapor. The corresponding effect on the model's finite-volume energy budget was accounted for by keeping track of the enthalpies of the exchanged gases. We apply this relative humidity nudging in every model level below 15 km, but not in the stratosphere.

To minimize the possibility of convective preconditioning (i.e., the probability that a developing cloud will grow through the moist detritus of a prior convective event), we should like to use a short τ in the free troposphere. However, if we nudge RH locally on too short a timescale near cloud base, we will never give clouds a chance to be born. Therefore, we specify an altitude-dependent τ given by

$$\tau(z) = \begin{cases} 1 \text{ minute} & z < 200 \text{ m} \\ 1 \text{ day} & 200\text{m} \leq z \leq 600 \text{ m} \\ \frac{10^7}{z^{1.35}} \text{ seconds} & 600 \text{ m} < z \end{cases}. \quad (9)$$

This profile of τ has the desirable properties of maintaining constant humidity in the subcloud-layer, giving clouds a chance to become saturated in the neighborhood of cloud base (~ 500 m), and quickly adjusting the RH of air outside of clouds to the target value in the free troposphere.

References

- Romps, D. M. (2015), MSE minus CAPE is the true conserved variable for an adiabatically lifted parcel, *Journal of the Atmospheric Sciences*, pp. 0–13.

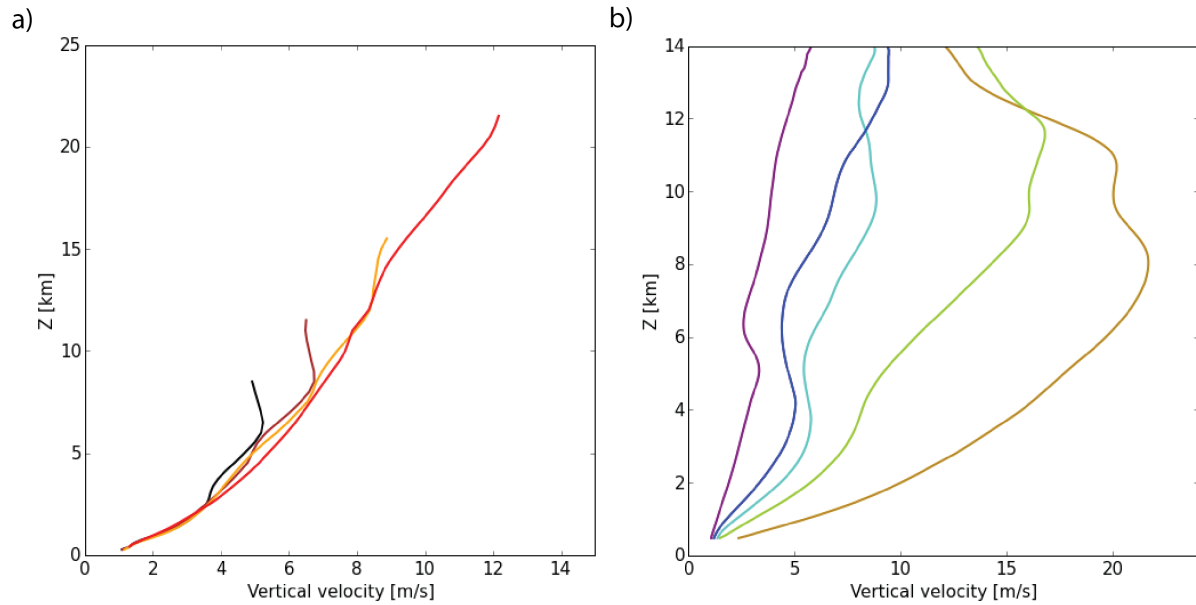


Figure S1. Profiles of mean vertical velocity in cloud updrafts in the CRM simulations from (a) the SST-warming experiment, and (b) the RH-varying experiment. Colors correspond to the set of SSTs and target free-tropospheric RH values as in Figures 2a and 4a of the main text. Note that (a) and (b) have different horizontal and vertical scales.